Journal of Biomolecular NMR, **12:** 407–415, 1998.
KLUWER/ESCOM

The solution structure of a gallium-substituted putidaredoxin mutant: GaPdx C85S

Thomas C. Pochapsky[a,*], Miklos Kuti[a] and Sophia Kazanis[b]
[a]*Department of Chemistry and* [b]*the Bioorganic Chemistry Program, Brandeis University, Waltham, MA 02254-9110, U.S.A.*

Received 1 May 1998; Accepted 11 June 1998

Key words: cytochrome P450, ferredoxin, paramagnetism, protein dynamics

Abstract

The Fe_2S_2 cluster of the ferredoxin putidaredoxin (Pdx) can be replaced by a single gallium ion, giving rise to a colorless, diamagnetic protein in which, apart from the metal binding site, the major structural features of the native ferredoxin are conserved. The solution structure of the C85S variant of gallium putidaredoxin (C85S GaPdx), in which a non-ligand cysteine is replaced by a serine, has been determined via multidimensional NMR methods using uniformly ^{15}N,^{13}C labeled samples of C85S GaPdx. Stereospecific assignments of leucine and valine methyl resonances were made using ^{13}C,^{1}H HSQC spectra obtained with fractionally ^{13}C-labeled samples, and backbone dihedral angle restraints were obtained using a combination of two-dimensional J-modulated ^{15}N,^{1}H HSQC and three-dimensional (HN)CO(CO)NH experiments. A total of 1117 NOE-derived distance restraints were used in the calculations, including 454 short range ($i - j \leq 3$), 456 long range ($i - j \geq 4$) interresidue restraints and 207 non-trivial intraresidue restraints. 97 ϕ and 55 χ_1 angular restraints were also included in the calculation of a family of 20 structures using a combined distance geometry-simulated annealing protocol. Most regions of the protein are well defined in the calculations, with an RMSD of 0.525 Å for backbone atoms excluding the metal binding loop (residues 34–48) and the last three C-terminal residues (residues 103–106). Where comparison is possible, these regions show an increase in dynamic behavior over the native protein, as does the loop containing residues 74–76. Structural and dynamic differences between native Pdx and GaPdx are discussed in relation to charge and packing of the metal binding site.

Introduction

Metal ions are ubiquitous in aqueous environments, and are often incorporated into folded proteins in either a structural or functional role. For NMR-based solution structure determinations, metal centers can pose challenges due to the lack of direct structural data from NMR concerning metal ligation geometry and spatial arrangement of nearby residues with respect to the metal. Paramagnetic metal centers in particular are problematic; sequential resonance assignments are often hampered by rapid nuclear relaxation, which limits the time available for polarization transfer and coupling evolution. In the course of our determination of the solution structure of the $Cys_4Fe_2S_2$ ferredoxin putidaredoxin (Pdx), we found that the paramagnetism of the iron-sulfur cluster broadened ^{1}H resonances sufficiently to prevent sequential assignments by standard homonuclear two-dimensional methods within ~8 Å of the cluster (Ye et al., 1992). Lacking a crystal structure for Pdx or for any closely homologous protein, it was necessary to model the metal center based on comparisons with ferredoxins with low (<10%) sequence homology (Pochapsky et al., 1994a). This prompted us to search for a diamagnetic metal ion that might substitute for the Fe_2S_2 cluster in Pdx. We subsequently described the reconstitution of Pdx with Ga^{+3}, which yielded a colorless diamagnetic protein (GaPdx) containing a single gallium atom in which the major structural features of the native protein are

*To whom correspondence should be addressed.

conserved (Kazanis et al., 1995). Recently, we described features of the metal binding site of GaPdx which were not observable in native Pdx and characterized local dynamics of the polypeptide backbone using heteronuclear relaxation measurements (Kazanis and Pochapsky, 1997). In that paper, we noted that the C85S variant of Pdx, in which a non-ligand cysteine residue has been mutated to a serine, also reconstitutes with gallium, yielding a product that is essentially identical to wild type GaPdx. However, the C85S reconstitution is somewhat cleaner than that of the wild type protein (presumably due to some misligation of the gallium ion in wild type protein). For this reason, we chose to characterize the C85S mutant of GaPdx exclusively in the current work. We now present a family of solution structures for C85S GaPdx calculated using NOE and dihedral angle restraints obtained from multidimensional NMR data.

Materials and methods

Sample preparation

Samples of uniformly ^{13}C,^{15}N- and ^{15}N-selectively labeled C85S GaPdx were prepared for NMR experiments as described previously (Lyons et al., 1996; Kazanis and Pochapsky, 1997). A sample of C85S GaPdx with stereospecific ^{13}C labeling of valine and leucine methyl groups was prepared as follows. The *lacI*$^{+}$ *E. coli* strain NCM533 was transformed with the plasmid pKM536 containing the appropriately modified *camB* gene behind the *lac* promoter. Single colonies were selected and grown overnight on LB media containing 100 mg/mL ampicillin. The cells were spun down and transferred to ampicillin-containing M9 media containing glycerol as sole carbon source. After acclimation, 50 mL of the culture was transferred to 1 L of M9 of which 10% of the glycerol present was uniformly ^{13}C-labeled (CIL). Each liter of media contained 0.33 g of ^{13}C-glycerol. Three liters of culture provided 0.2 mL of a 2 mM sample of fractionally labeled GaPdx after reconstitution. Induction, cell harvest, protein purification and reconstitution with gallium were accomplished as described previously (Kazanis and Pochapsky, 1997).

NMR spectroscopy

Most of the NMR experiments used for sequential assignments of ^{1}H, ^{13}C and ^{15}N resonances of C85S GaPdx as well as those used to obtain NOE and couplings for angular restraints were described previously (Kazanis and Pochapsky, 1997). All experiments were performed on a Bruker AMX-500 spectrometer equipped with a three-channel Acustar pulsed field gradient amplifier and *x*, *y*, *z*-gradient triple resonance inverse detection probehead. The AMX-500 operates at 500.13 MHz, 50.68 MHz and 125.76 MHz for ^{1}H, ^{15}N and ^{13}C respectively. All ^{1}H chemical shifts are referenced to external DSS using the water signal as internal reference. ^{15}N chemical shifts are referenced to external liquid ammonia using the ^{1}H resonance of H_2O (Live et al., 1984) and ^{13}C chemical shifts are reported relative to the methyl resonance of external TSP (Bax and Subramanian, 1986). Quadrature detection in the indirect dimension was achieved for all experiments using either hypercomplex or time proportional phase incrementation (TPPI) data acquisition. Either GARP-1 (Shaka et al., 1985) or WALTZ-16 (Shaka et al., 1983) composite pulse decoupling schemes were used for broadband decoupling of heteronuclei during acquisition. Data processing and analysis was performed using the FELIX 97.0 software package operating on a Silicon Graphics O2 work station.

A combination of short (35 ms) mixing time TOCSY-^{1}H,^{15}N HSQC and HNHB data obtained with uniformly ^{15}N-labeled samples were used to make stereospecific assignments of β-methylene protons and to obtain estimates for χ_1 angles (Clore and Gronenborn, 1991; Archer et al., 1991). These experiments were performed using published pulse sequences and the same conditions, settings and processing methods described previously (Kazanis and Pochapsky, 1997). In order to obtain stereospecific methyl assignments for valine and leucine, ^{1}H,^{13}C-HSQC experiments were performed at 298 K and at 290 K without ^{13}C decoupling during acquisition with WATERGATE-type water suppression (Bodenhausen and Ruben, 1980; Piotto et al., 1992) using a fractionally ^{13}C-labeled sample prepared as described above. These experiments exhibit splittings in the ^{13}C dimension which identify couplings between neighboring ^{13}C-labeled carbons, enabling stereospecific assignment of valine γ- and leucine δ-CH_3 resonances (Neri et al., 1989, 1990). For these high-resolution non-constant time experiments, 1024 complex points were collected during t_2 for each of 2048 values of t_1. Quadrature detection in the t_1 dimension was obtained using TPPI. Spectral widths of 8440 Hz (^{13}C, t_1) and 6024 Hz (^{1}H, t_2) were used.

In order to obtain estimates of backbone φ dihedral angles, $^{3}J_{C'C'}$ carbonyl couplings were measured via

an (HN)CO(CO)NH experiment (Grzesiek and Bax, 1997) using a uniformly ^{15}N,^{13}C-labeled sample of GaPdx (Figure 1). The experiment was performed at 298 K, with the ^{15}N carrier frequency set to 120 ppm. The ^{13}C frequency was set in the carbonyl region (177.2 ppm) and low-power on- and off-resonance square pulses were used to selectively excite ^{13}C resonances in the carbonyl and C_α regions, respectively. 58 (t_1 ^{13}C) × 45 (t_2 ^{15}N) × 512 (t_3 ^{1}H) complex points were collected with acquisition times of 27 ms (t_1 ^{13}C), 27 ms (t_2 ^{15}N) and 85 ms (t_3 ^{1}H). Isotropic mixing of the ^{13}C carbonyl resonances was accomplished using a DIPSI-3 sequence (Shaka et al., 1988), with an isotropic mixing period of 115 ms. Water suppression was achieved using the WATERGATE sequence. Quadrature detection in the t_1 and t_2 dimensions was accomplished using the States-TPPI method. 32 fids were collected for each increment, resulting in an experimental duration of 4 days. The fids were 50% truncated and apodized with a squared cosine bell in the t_3 dimension. In the t_2 and t_1 dimensions the data were extended by linear prediction to 60 and 80 points, respectively, and apodized with a 70° shifted sine bell. The resulting data matrix contains 128 (ω_1) × 128 (ω_2) × 512 (ω_3) points, with spectral widths of 2200 Hz (ω_1 ^{13}C) × 1700 Hz (ω_2^{15}N) × 6048 Hz (ω_3^{1}H).

Structural calculations

NOE restraints for structural calculations were obtained from homonuclear 2D flipback NOESY and 3D ^{13}C- and ^{15}N-edited NOESY experiments as described previously (Kazanis and Pochapsky, 1997). A mixing time of 70 ms was used for all NOESY experiments, since examination of NOE buildup curves indicated that NOE cross peaks obtained at this mixing time are essentially free of spin diffusion effects. Strong NOEs were assigned distances of ≤3 Å, medium NOEs ≤4 Å, and weak NOEs ≤5 Å, with an allowed error of +0.3 Å without energy penalty. φ dihedral angle restraints were obtained from NH–C_αH coupling constants as obtained from *J*-modulated ^{1}H,^{15}N HSQC experiments or from backbone C′–C′ carbonyl carbon couplings as measured using the (HN)CO(CO)NH experiment. In cases where good agreement (≤10°) was obtained for a φ dihedral angle from both methods, an angular variation of ±20° was permitted from the assigned dihedral angle without energetic penalty. If data from only one experiment was available or the results from one or the other ambiguous, a variation of ±40° was permitted without energetic penalty. Although in no case did the data from the two experiments contradict each other, the carbonyl coupling data generally gave less ambiguous results. As neither experiment distinguishes between positive and negative values of φ, it was necessary to test both values for several residues in order to determine which best fit the observed data (vide infra).

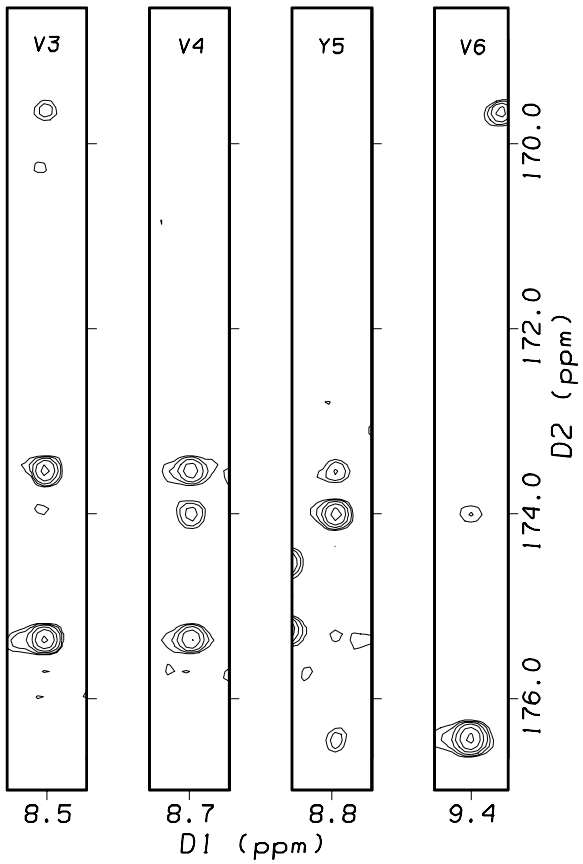

Figure 1. Strips from planes in the (HN)CO(CO)NH experiment on C85S GaPdx corresponding to the ^{15}N chemical shifts of the residues noted, showing peaks resulting from coupling between carbonyl carbons. Relative peak intensities correspond to the efficiency of coherence transfer during the spin lock, a function of backbone conformation as reflected by $^3J_{C'C'}$ (Gresziek and Bax, 1997).

Structural calculations were performed on a Silicon Graphics O2 workstation running XPLOR 3.851 (A. Brünger, Yale University). A modification of the combined distance geometry-simulated annealing protocol of Nilges et al. was used for the calculations (Nilges et al., 1988). A .psf file was generated for GaPdx using the sequence of C85S putidaredoxin and including a patch which deletes the γ-hydrogen from the four cysteines that ligate the metal center (C39,

C45, C48 and C86) and forms bonds between the Sγ of those residues and Ga^{+3} metal ion. Ga-S bond lengths were set at 2.28 Å, while the ligation of the Ga ion was set loosely to be tetrahedral via S-Ga-S bond angle restraints and distance restraints between the cysteinyl Sγ atoms. Both the Ga-S bond length and geometry of the Ga coordination sphere are based on EXAFS data for GaPdx, which are consistent with S_4 tetrahedral ligation distorted toward square planar (Kazanis et al., 1995). The stereochemistry of gallium ligation was not defined by improper angles, and so was free to assume the lowest energy configuration during the calculations. A first round of distance geometry calculations were performed as follows. A structure generated from the published solution structure of Pdx was used as a template for pseudoatom corrections and for configurational constraints. A set of sub-structures was then generated using the distance geometry routine (bound smoothing, substructure embedding and regularization). Sub-structures were tested for the correct enantiomer first by comparison of the energies due to violations of improper angles defining chirality around stereocenters in the protein with those generated by reflection of the substructure along the x-axis, and then by comparison of the substructure and its reflection with a reference structure generated from the published structure of native Pdx (PDB reference 1PUT). Those substructures which passed the test for the correct enantiomer and were consistent with the applied NOE and dihedral angle restraints were then subjected to simulated annealing for further refinement. The template structure was used to generate all atoms and local idealized geometries for the embedded substructures. The resulting structures were then energy-minimized with respect to bonds, van der Waals contacts, dihedral angles and NOE restraints prior to simulated annealing. In order to account for non-stereospecific assignments, NOEs to aromatic protons and to equivalent protons of methyl groups, r^{-6} averaging of NOE-defined distances was used in all structural calculations. High temperature annealing (2000 K) was performed for 1000 steps ($\Delta t = 3$ fs), during which improper angles defining chirality and planarity of peptide bonds and aromatic rings were slowly introduced and van der Waals interactions increased. No electrostatic terms were used in the calculations. The structures were then cooled to a final temperature of 100 K over 1000 3 fs steps and minimized with respect to bond lengths, bond angles, improper angles, van der Waals interactions, NOE and dihedral restraints. The structures shown here exhibit no NOE violation greater than 0.5 Å, and no dihedral angle violation greater than 5°.

Results

The statistics of the family of twenty structures of C85S GaPdx presented here (Figure 2) are given in Table 1. With two exceptions, all non-glycinyl residues exhibit ϕ angles for the polypeptide backbone in the allowed negative ϕ angle region of ϕ–ψ space. The two exceptions, Ala 43 and Glu 77, were constrained to the additional allowed region (positive ϕ angle near 60°, ψ angle near 40°). Both of these are consistent with results of the (HN)CO(CO)NH experiment and are observed for the positionally homologous residues (Leu 50 and Gly 83) in the recently solved crystal structure of a truncated bovine adrenodoxin (Müller et al., 1998). The positive ϕ angle at Glu 77 was initially observed in low-energy structures when dihedral restraints were removed from Glu 77. The consistency of this angle with observed intra- and intraresidue NOEs involving residue 77, with (HN)CO(CO)NH data, and with the Adx structure was such that this angle was constrained as positive for the calculation of the presented structures. Both positive and negative ϕ angles consistent with the results of the HNCO(CO)NH experiments were tested at residue 43, with the positive angle yielding structures more consistent with observed NOEs and other angles in the metal binding loop. In order to reduce calculation time, residues consistently giving rise to a positive ϕ angle in the additional allowed region of ϕ–ψ space were restrained with the appropriate ψ angle ($+40° \pm 20°$) for the final structural calculations.

Features of the GaPdx structure and comparison with native Pdx and bovine adrenodoxin (Adx)

As noted previously, the global fold of native (Fe-containing) Pdx is conserved in the Ga-reconstituted protein (Kazanis and Pochapsky, 1997) (Figure 3). A figure comparing the backbones of native and GaPdx is presented in our previous publication. All major secondary structural features observed in the native protein are also observed in GaPdx, and for the most part the pattern of slowly exchanging amide protons in GaPdx mirrors the patterns observed in native Pdx. The GaPdx structure also offers the first structural information concerning residues which interact directly with the metal center. For example, in all crystal structures of ferredoxins solved to date, there is

Table 1. Statistics for the 20 C85S GaPdx structures presented

NOE restraints			
	Non-trivial intraresidue	Short range ($i - j \leq 3$)	Long range ($i - j \geq 4$)
Involving metal binding loop residues (34–48)	6	18	33
Involving C-terminal residues (103–106)	3	11	3
Overall	207	454	456
Dihedral restraints			
97	C'–N–C_α–C'(ϕ) restraints		
55	H_α–C_α–C_β–H_β (χ_1) restraints		
4	N–C_α–C'–N (ψ) restraints (40° ± 20° on residues with positive ϕ angles in additional allowed region; see text)		
RMSDs (Å)			
		Backbone heavy atoms	All heavy atoms
Excluding metal binding loop residues (34–48) and C-terminal residues (103–106)		0.525	0.882
Overall		0.832	1.260

Figure 2. Superposition of 20 structures of C85S GaPdx generated as described in the text. Most variability is seen in the metal binding loop (top center), the C-terminal residues (top left-center) and residues Val 74–Ala 76 (top left). Backbone RMSDs are 0.525 Å for backbone heavy atoms excluding residues 34–48 and 103–106, and 0.832 Å for when all backbone heavy atoms are included. RMSDs of 0.882 Å are observed for all heavy atoms when residues 34–48 and 103–106 are excluded, and 1.260 Å when all residues are included. Fits and the stereofigure were both generated using MOLMOL 2.5.1 (ETH Zürich).

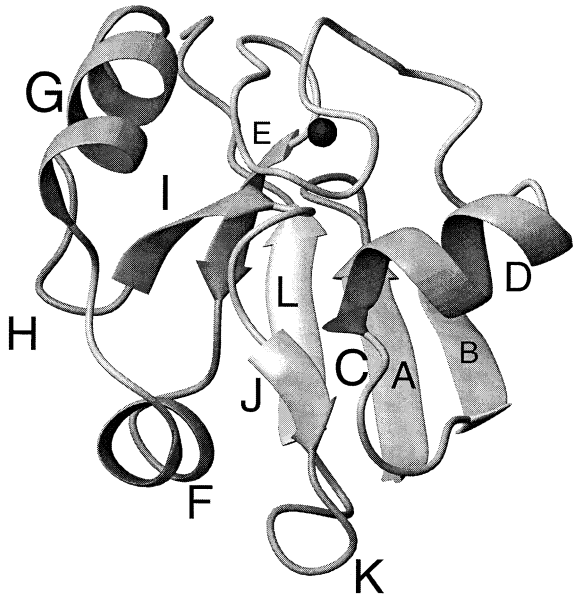

Figure 3. Secondary structural features and global fold of GaPdx. The view is approximately the same as in Figure 2. Structural features are identified by letter: **A** Lys 2–Ser 7; **B** Arg 12–Val 17, **C** Val 21–Ser 22; **D** Leu 23–Asp 30; **E** Val 50–Asn 53; **F** Ala 55–Val 60; **G** Gln 64–Cys 73; **H** Lys 79–Ser 82; **I** Arg 83–Ser 85; **J** Ile 88–Met 90; **K** Thr 91–Leu 94; **L** Ile 97–Pro 102. The gallium atom is represented by a dark sphere (top center). The figure was generated using MOLMOL 2.5.1 (ETH Zürich).

considerable hydrogen bonding observed between the sulfur ligands of the iron atoms and backbone amide protons. These hydrogen bonds appear to stabilize the local geometry and may be involved in modulating the redox potential of the cluster. The backbone polypeptide conformation generated by NOE and dihedral angle restraints on residues in the metal binding site of GaPdx results in many backbone amide hydrogens facing toward the metal center, including those of all four of the cysteinyl ligands (Cys 39, Cys 45, Cys 48 and Cys 86) as well as those of Gly 41, Ser 42, Ala 43 and Ser 44. Other functionality in close proximity to the metal center include the O_γ of Thr 47, the O_γ of Ser 85 and the S_δ of Met 24 (Figure 4). These atoms could also potentially be involved in modulating the redox behavior of the metal cluster in native Pdx. Differences in fine structure of EXAFS data from wild-type and C85S GaPdx support the notion that the γ-atom of residue 85 is involved in second-sphere interactions with the metal center (Kazanis et al., 1995).

There are also differences between native Pdx and GaPdx that underscore the importance of the interactions between the polypeptide and bound metal to overall protein stability and folding. The most noticeable of these differences is the stability of the C-terminal cluster, a compact region of the protein which in native Pdx is formed by the side chains of His 49, Tyr 51, Ser 82, Leu 71, Val 74, Ala 76, Leu 78, Pro 102, Arg 104 and Trp 106 (Pochapsky et al., 1994b). The GaPdx structure shows that the side chains of Met 70 and Leu 84 also contribute to the formation of the cluster, these residues also being adjacent to the metal cluster binding site (Figure 4). The C-terminal cluster is a distinct feature of the class of ferredoxins that transfer electrons to monooxygenases, and similar regions are seen in the recently published crystal structure of bovine adrenodoxin (Muller et al., 1998) and in the solution structure of terpredoxin (Mo and Pochapsky, unpublished results). The cluster is held together by a network of hydrogen bonds and hydrophobic interactions, and is responsive to changes in the oxidation state of the metal cluster, both in terms of amide proton exchange rates and chemical shifts (Pochapsky et al., 1994b; Lyons et al., 1996). One residue in this cluster, Trp 106, has been identified as critical for binding to the physiological redox partner of Pdx, cytochrome $P450_{cam}$ (Davies and Sligar, 1992), and we have suggested that redox-dependent changes in the C-terminal cluster region may help modulate the binding of Pdx to redox partners as a function of oxidation state (Lyons et al., 1996; Pochapsky et al., 1996).

NOE data confirm that the C-terminal cluster remains intact in GaPdx. It is, however, considerably more dynamic than in the native protein. The four C-terminal residues (Asp 103 to Trp 106) form an integral part of the C-terminal cluster in native Pdx, but are clearly disordered in GaPdx (Figure 2) and Trp 106 no longer exhibits the interresidue NOEs from the indole side chain to Val 74 that are observed in the native protein. Except for a few weak NOEs oberved between Arg 104 and Ala 76, residues Asp 103–Trp 106 are not restrained to the remainder of the structure in GaPdx structural calculations. Other parts of the C-terminal cluster are also affected by the metal substitution. The hydroxyl proton of Ser 82 in native Pdx exchanges slowly enough with solvent for coupling with the $C_\beta H_2$ protons to be distinguished in double quantum correlation spectra (Pochapsky and Ye, 1991). In GaPdx, the Ser 82 OH proton is no longer observed. The $N_\delta H$ imidazole proton of His 49, which is strongly shifted downfield in the native protein, is also not observed in GaPdx. Finally, the ^1H resonances of Val 74, Thr 75 and Ala 76 are broadened in GaPdx

relative to their line widths in the native protein, indicating that dynamic processes are taking place in this region on a time scale of tens of milliseconds. Similar broadening is observed for ^{1}H resonances of some residues in the metal binding loop, especially (but not exclusively) for Cys 45 and Thr 47, both of which are in close proximity to the metal center and to the C-terminal cluster. Taken together, these observations suggest that the close packing of residues in this region is perturbed by the replacement of the Fe_2S_2 cluster with a single gallium atom. Net charge may also be be important, as the Fe_2S_2 cluster cycles between a net $+2/+1$ charge while the gallium ion has a fixed charge of $+3$. Depending upon their orientation with respect to the metal center, hydrogen bonds could alternatively be weakened or strengthened with the change in charge, providing a mechanism whereby changes in charge density at the metal center could be reflected in dynamic changes in the rest of the protein (Pochapsky et al., 1998). Finally, the change in the orientation of the ligands may introduce structural perturbations that result in imperfect packing of residues in the vicinity of the metal binding site. Free energy perturbation simulations currently in progress in conjunction with structural calculations on the native Pdx may shed some light on this possibility.

The metal cluster binding loop of GaPdx also exhibits considerable flexibility in the structural calcuations (Figure 2). The residues which make up the loop are small and surface exposed, with little in the way of steric constraints imposed by side chain packing. In the absence of a complete Fe-S cluster, steric restraints on residues in the loop are reduced even further. This is reflected in the relative paucity of NOEs to residues in the loop; while residues in the rest of the protein (excluding the last three residues, Asp 103–Trp 106) are restrained by an average of 12.5 NOEs per residue, those in the loop (residues 34 to 48) are restrained by an average of only 4.1 NOEs per residue. As such, imposed dihedral angle restraints as determined from J-coupling measurements are at least as important as NOE restraints in determining the conformation of loop residues in the structures presented here.

The crystal structure of a protein sequentially and functionally related to Pdx, oxidized bovine adrenodoxin, was recently solved to 1.85 Å (Müller et al., 1998), and represents the first crystal structure to be solved for this class of ferredoxin. The similarities between Adx and Pdx prompt a brief comparison between their structures. Both show the same folding topology, with minor differences in secondary structure. Structural alignment (excluding the C-terminus and the metal cluster binding loop), clearly indicate that the two proteins have similar structures (Figure 5). It is also seen that many of the specific features of Pdx and GaPdx discussed here and in previous papers have close counterparts in the Adx structure. The C-terminal cluster, which is implicated in redox partner recognition for both proteins, exhibits very similar organization in Pdx and in Adx (Pochapsky et al., 1994b; Müller et al., 1998). The largest differences are observed in the region of the polypeptide immediately to the N-terminal end of the metal binding loop, residues 32 to 38 in Pdx. In GaPdx, there is a turn-like feature involving residues 32–35, while the same region in Adx is more extended. This may be due to the difference in the positions of the aromatic residues in this region of each protein. Although the side chains of Tyr 33 (GaPdx) and Phe 43 (Adx) occupy essentially identical positions in their respective structures, their backbone positions are not homologous, and different polypeptide conformations appear to be required in order to reach the correct set of folded contacts.

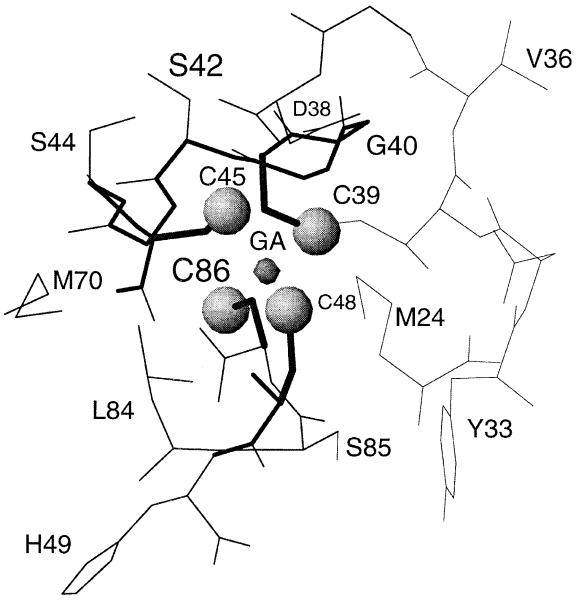

Figure 4. Structural features of the metal binding site of GaPdx, as viewed from approximately the same orientation as in Figures 2 and 3. Sγ sulfurs of the four ligating cysteines (Cys 39, 45, 48 and 86) are shown as large spheres. The Ga ion is shown as a smaller sphere. The side chain bonds of the ligating cysteines are shown in the heaviest lines. Backbone connectivities for residues in the metal binding loop (Cys 39 through Cys 45) are shown with lines of intermediate width. His 49, Met 70 and Leu 84 interact with the C-terminal cluster, while Met 24 is found in helix D (see Figure 4). The figure was generated using MOLMOL 2.5.1 (ETH Zürich).

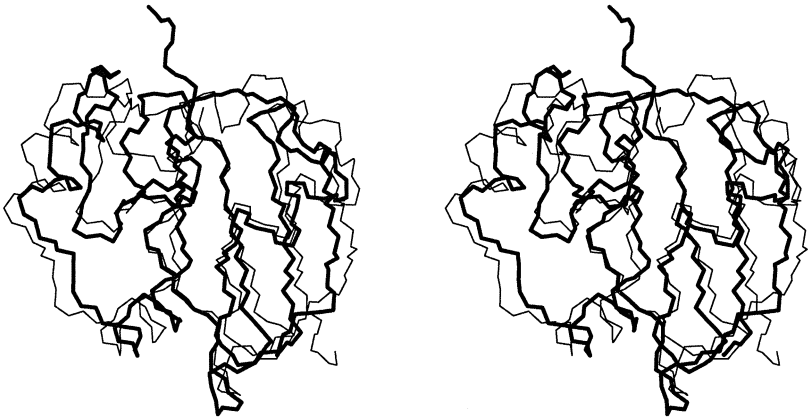

Figure 5. Backbone overlay of the mean structure of C85S GaPdx (heavy lines) onto that of bovine adrenodoxin (Adx) (Müller et al., 1998). Alignment was made from backbone atoms of residues 5–31, 49–70, and 76–83 (Pdx) to residues 11–37, 56–77 and 82–89 (Adx), resulting in an RMSD of 1.64 Å. The fit and stereodrawing were both generated using MOLMOL 2.5.1 (ETH Zürich).

Conclusions

In general, Fe_2S_2 ferredoxins require the presence of a metal center in order for tertiary structure to be detectable by NMR methods. This indicates that the formation and incorporation of the metal cluster is an essential step in stabilizing the tertiary fold of the nascent ferredoxin, and that incorporation of the metal center is properly considered as a late (perhaps final) step in folding. Comparison of metal reconstitutions of different ferredoxins may give insight into how particular types of metal centers are selected for by the nascent protein. Recently, the reconstitution of the $Cys_4Fe_2S_2$ ferredoxin from the cyanobacterium*Anabaena* with a complete Ga_2S_2 cluster was described (Vo et al., 1997). The conditions described for that reconstitution differ only minimally from those used for GaPdx, but in that case, sulfide ion was essential to the reconstitution, while the same mononuclear product is obtained for gallium reconstitution of Pdx regardless of whether sulfide ion is present or not (Kazanis et al., 1995). We have reconstituted Pdx using precisely the reported conditions of Vo et al., and still obtained the mononuclear product as in our original work. We have observed that the Ga^{+3}reconstitution of terpredoxin, a ferredoxin with ∼50% sequence identity to Pdx, also appears to give a mononuclear product using the conditions of Vo et al., and is not sulfide dependent (Huaping Mo, unpublished results). However, Vo et al. noted that Ga_2S_2 cluster incorporation is observed for a ferredoxin from *Trichomonas vaginalis*, so complete cluster incorporation is not unique to the *Anabaena* ferredoxin.

The reconstituted *Anabaena* ferredoxin was reported to be structurally and dynamically very similar to the native protein, as measured by chemical shifts and amide proton exchange rates. Interestingly, ten of the amide protons which were newly identified in the diamagnetic form of the *Anabaena* ferredoxin were reported to be slowly exchanging in D_2O, suggesting that the metal binding loop in Ga-reconstituted *Anabaena* ferredoxin is considerably less dynamic than in GaPdx, and that the Ga-S cluster stabilizes the *Anabaena* ferredoxin structure to nearly the same extent as the native Fe-S cluster. On the other hand, as described here and previously (Kazanis and Pochapsky, 1997), the metal binding loop of GaPdx is fairly flexible, consisting mostly of glycines and hydrophilic amino acids with small chains. What structural integrity this region has is almost entirely due to the ligation of the metal ion itself. The metal binding loop of Pdx, (D-C-G-G-S-A-S-C-A-T-C) is one residue longer and contains two more glycines than the *Anabaena* ferredoxin loop (S-C-R-A-G-A-C-S-T-C), so is probably more flexible and may be better able to adjust to the steric requirements of binding a single metal ion. Site-directed mutagenesis experiments are currently under way to test this hypothesis. As GaPdx is stable to the presence of iron and sulfide and does not require excess gallium ion to maintain stability, we speculate that GaPdx may represent a kinetically trapped late folding intermediate, in which the normal sequence of incorporation of metal and sulfide to form

the metal cluster is interrupted by the tight binding of a single gallium ion.

Supplementary material

Stereospecific ^{1}H, ^{13}C and ^{15}N assignments for GaPdx are available from the authors, and have been deposited in the BioMagResBank (accession number 4149). A set of 20 structures of GaPdx has been deposited in the PDB database (1GPX), and is available upon request from the authors.

Acknowledgements

This work was supported in part by a grant from the U.S. National Institutes of Health (GM44191, TCP). The authors thank Jennifer Heymont for help in setting up the structural calculations, and Dr Jürgen Müller of the Max Delbruck Institute (Berlin) for access to the coordinates of the bovine adrenodoxin crystal structure. SK acknowledges financial support from the NSERC (Canada) and FCAR (Quebec) graduate fellowship programs.

References

Archer, S.J., Ikura, M., Torchia, D.A. and Bax, A. (1991) *J. Magn. Reson.*, **95**, 636–641.

Bax, A. and Subramanian, S. (1986) *J. Magn. Reson.*, **67**, 565–569.

Bodenhausen, G. and Ruben, D.J. (1980) *Chem. Phys. Lett.*, **69**, 185–188.

Clore, G.M. and Gronenborn, A. (1991) *Prog. NMR Spectrosc.*, **23**, 43–92.

Davies, M.D. and Sligar, S.G. (1992) *Biochemistry*, **31**, 11383–11389.

Grzesiek, S. and Bax, A. (1997) *J. Biomol. NMR*, **9**, 207–211.

Kazanis, S., Pochapsky, T.C., Barnhart, T.M., Penner-Hahn, J.E., Mirza, U.A. and Chait, B.T. (1995) *J. Am. Chem. Soc.*, **117**, 6625–6626.

Kazanis, S. and Pochapsky, T.C. (1997) *J. Biomol. NMR*, **9**, 337–346.

Live, D., Davis, D.G., Agosta, W.C. and Cowburn, D. (1984) *J. Am. Chem. Soc.*, **106**, 1939–1941.

Lyons, T.A., Ratnaswamy, G. and Pochapsky, T.C. (1996) *Protein Sci.*, **5**, 627–639.

Müller, A., Müller, J.J., Muller, Y.A., Uhlmann, H., Bernhardt, R. and Heinemann, U. (1998) *Structure*, **6**, 269–280.

Neri, D., Otting, G. and Wüthrich, K. (1990) *J. Am. Chem. Soc.*, **112**, 3663–3665.

Neri, D., Otting, G. and Wüthrich, K. (1990) *Tetrahedron*, **46**, 3287–3296.

Neri, D., Szyperski, T., Otting, G. Senn, H. and Wüthrich, K. (1989) *Biochemistry*, **28**, 7510–7516.

Nilges, M., Clore, G.M. and Gronenborn, A.M. (1988) *FEBS Lett.*, **239**, 317–324.

Piotto, M., Saudek, V. and Sklenar, V. (1992) *J. Biomol. NMR*, **2**, 661–665.

Pochapsky, T.C. and Ye, X.M. (1991) *Biochemistry*, **30**, 3850–3856.

Pochapsky, T.C., Ye, X.M., Ratnaswamy, G. and Lyons, T. A. (1994a) *Biochemistry*, **33**, 6424–6432.

Pochapsky, T.C., Ratnaswamy, G. and Patera, A. (1994b) *Biochemistry*, **33**, 6433–6441.

Pochapsky, T.C., Lyons, T.A., Kazanis, S., Arakaki, T. and Ratnaswamy, G. (1996) *Biochimie*, **78**, 723–733.

Pochapsky, T.C., Arakaki, T., Jain, N., Kazanis, S., Lyons, T.A., Mo, H., Patera, A., Ratnaswamy, G. and Ye, X. (1998) in *Structure, Motion, Interaction and Expression of Biological Macromolecules* (R.H. Sarma and M. H. Sarma, Eds), Adenine Press.

Shaka, A.J., Keeler, J., Frenkiel, T. and Freeman, R. (1983) *J. Magn. Reson.*, **52**, 335–338.

Shaka, A.J., Barker, P.B. and Freeman, R. (1985) *J. Magn. Reson.*, **64**, 547–552.

Shaka, A.J., Lee, C.J. and Pines, A. (1988) *J. Magn. Reson.*, **77**, 274–293.

Vo, E., Wang, H.C. and Germanas, J.P. (1997) *J. Am. Chem. Soc.*, **119**, 1934–1940.

Ye, X. M., Pochapsky, T.C. and Pochapsky, S.S. (1992) *Biochemistry*, **31**, 1961–1968.